

# Geometric characterization of anomalous Landau levels of isolated flat bands

Yoonseok Hwang,<sup>1,2,3</sup> Jun-Won Rhim,<sup>1,2,\*</sup> and Bohm-Jung Yang<sup>1,2,3,†</sup>

<sup>1</sup>*Center for Correlated Electron Systems,*

*Institute for Basic Science (IBS), Seoul 08826, Korea*

<sup>2</sup>*Department of Physics and Astronomy,*

*Seoul National University, Seoul 08826, Korea*

<sup>3</sup>*Center for Theoretical Physics (CTP),*

*Seoul National University, Seoul 08826, Korea*

(Dated: June 13, 2022)

## Abstract

Landau levels of a band are conventionally believed to be bounded by its upper and lower band edges at zero magnetic field so that no Landau level is expected to appear in the gapped regions of the original band structure. Two notable examples evading this expectation are topological bands with quantized invariants and flat bands with singular band crossing. Here we introduce a distinct class of flat band systems in which an isolated flat band exhibits anomalous Landau level spreading (LLS) outside the zero-field energy bounds. In particular, we demonstrate that the LLS is determined by the cross-gap Berry connection measuring the wave function geometry of multi-bands. Moreover, we find that symmetry puts strong constraints on the LLS of flat bands. Namely, the LLS shows a quadratic magnetic field dependence in systems with space-time-inversion symmetry while it completely vanishes when the system respects chiral symmetry. Also, when the system respects time-reversal or reflection symmetries at zero magnetic field, the maximum and minimum values of the LLS have the same magnitude but with opposite signs. Our general mechanism for the LLS of flat bands reveals the fundamental role of wave function geometry in describing anomalous magnetic responses in solids.

---

\* [phyruth@gmail.com](mailto:phyruth@gmail.com)

† [bjyang@snu.ac.kr](mailto:bjyang@snu.ac.kr)

Geometry of Bloch wave functions, manifested in the quantities such as Berry curvature and Berry phase, is a central notion in modern description of condensed matter. Due to the significant role of the wave function geometry in describing the fundamental properties of solids, finding efficient methods of measuring it has been considered as a quintessential problem in solid state physics. In this respect, examining the Landau level spectrum has received a particular attention, as one of the most efficient and convenient methods for detecting the geometric properties of Bloch states.

In general, computing Landau levels of electrons in periodic crystals is a complicated quantum mechanics problem, from which it is hard to get an intuitive understanding of underlying physics. On the other hand, the semiclassical approach based on the Onsager's quantization rule provides an efficient and intuitive method for describing Landau levels in weak field limit from simple band structure information. The Onsager's semiclassical quantization rule is given by

$$S_0(\epsilon) = \frac{2\pi eB}{\hbar} \left( n + \frac{1}{2} - \frac{\gamma_{\epsilon,B}}{2\pi} \right), \quad (1)$$

where  $S_0(\epsilon)$  is the area of a closed semiclassical orbit at the energy  $\epsilon$  in momentum space,  $B$  is magnetic field,  $e$  is the electric charge,  $\hbar$  is the reduced Planck constant,  $n$  is a non-negative integer, and  $\gamma_{\epsilon,B}$  is the quantum correction from Berry phase, orbital magnetization, and so on [1–5]. In conventional parabolic bands, Eq. (1) correctly gives the well-known equally-spaced Landau levels. Also, in graphene with relativistic energy dispersion, Eq. (1) successfully predicts the  $\sqrt{nB}$  dependence of the Landau levels, and the existence of the zero-energy Landau level manifesting the  $\pi$ -Berry phase of massless Dirac particles [6, 7]. Later, this semiclassical approach is generalized further to the cases with an arbitrary strength of magnetic field [8] where the zero-field energy dispersion in Eq. (1) is replaced by the magnetic band structure with  $B$  linear quantum corrections.

In usual dispersive bands where the  $B$  linear quantum corrections are negligible in weak field limit, the Onsager's semiclassical approach in Eq. (1) predicts that the Landau levels are developed in the energy interval bounded by the upper and lower band edges of the zero-field band structure. Thus, the Landau levels appearing in gapped regions away from the zero-field energy bounds can be considered anomalous. Up to now, few examples exhibiting anomalous Landau levels have been reported. One famous example is the Landau levels of a Chern band which appear in an adjacent energy gap at zero-field. Similar behavior was also recently predicted in fragile topological bands characterized by nonzero Euler numbers [9–11]. More recently, it was shown

that anomalous Landau levels also appear in singular flat bands [12, 13] where a flat band is crossing with another parabolic band at a momentum [14]. Interestingly, it is found that the Landau levels of a singular flat band appear in the energy region with vanishing density of states at zero magnetic field. Moreover, the total energy spreading of the flat band's Landau levels, dubbed the Landau level spreading (LLS), is solely determined by a geometric quantity, called the maximum quantum distance which characterizes the singularity of the relevant Bloch wave function [14].

In this work, we propose a distinct class of flat-band systems that exhibit anomalous Landau level structures. The flat band we consider is isolated from other bands by a gap, which we call an isolated flat band (IFB). An IFB is generally non-singular as well as topologically trivial [15–17], so that it does not belong to any category of the systems exhibiting anomalous Landau levels discussed above. Unexpectedly, however, it is found that the Landau levels of IFBs are anomalous, that is, unbounded by the original band structure at zero magnetic field.

In fact, the Onsager's semiclassical quantization rule in Eq. (1) generally does not work in flat bands, unless the  $B$  linear quantum corrections are properly included. This is because there are infinitely many semiclassical orbits allowed so that  $S_0(\epsilon)$  cannot be uniquely determined. Interestingly, after taking into account the  $B$  linear quantum corrections, we find that an IFB generally exhibits anomalous LLS, and the upper and lower energy bounds for the LLS are determined by the cross-gap Berry connection defined as

$$A_i^{nm}(\mathbf{k}) = i\langle u_n(\mathbf{k}) | \partial_i u_m(\mathbf{k}) \rangle \quad (n \neq m), \quad (2)$$

where  $u_n(\mathbf{k})$  is the periodic part of the Bloch wave function of the  $n$ -th band [18]. This is a multi-band extension of the conventional Abelian Berry connection and describes inter-band couplings. Let us note that, unlike the Abelian Berry connection defined for a single band, the cross-gap Berry connection  $A_i^{nm}(\mathbf{k})$  ( $n \neq m$ ) is gauge-invariant. We will show that the LLS of an IFB is given by the product of the  $x$  and  $y$  components of the cross-gap Berry connection between the flat band and other bands weighted by their energy. The LLS of an IFB is strongly constrained by the symmetry of the system, which is demonstrated in various flat band models including the Lieb and the Tasaki models as well as the model describing twisted bilayer graphene (see Results and Supplementary Note 3). We believe that our theory provides a new insight for the fundamental role of wave function geometry in describing the Landau levels of flat bands.

## Results

## Modified band dispersion and the Landau level spreading

The original Onsager's semiclassical approach predicts IFBs inert under external magnetic field, and thus it cannot explain the LLS of IFBs. On the other hand, the *modified semiclassical approach* developed by M.-C. Chang and Q. Niu [8] can resolve this problem. Contrary to the Onsager's approach, where the band structure at zero magnetic field  $\varepsilon_n(\mathbf{k})$  is used to define the closed semiclassical orbits and the corresponding area  $S_0(\epsilon)$ , the modified semiclassical approach employs the modified band structure given by

$$E_{n,B}(\mathbf{k}) = \varepsilon_n(\mathbf{k}) + \mu_n(\mathbf{k})B, \quad (3)$$

where  $\mathbf{B} = B\hat{z}$  is the magnetic field,  $n$  is the band index, and  $\mu_n(\mathbf{k})$  is the orbital magnetic moment of the  $n$ -th magnetic band in the  $z$ -direction arising from the self-rotation of the corresponding wave packet [8]. The explicit form of  $\mu_n(\mathbf{k})$  is

$$\mu_n(\mathbf{k}) = \frac{e}{\hbar} \text{Im} \langle \partial_x u_n(\mathbf{k}) | [\varepsilon_n(\mathbf{k}) - H(\mathbf{k})] | \partial_y u_n(\mathbf{k}) \rangle, \quad (4)$$

where  $H(\mathbf{k})$  is the Hamiltonian in momentum space. Hence, the second term on the right-hand side of Eq. (3) indicates the leading energy correction from the orbital magnetic moment coupled to the magnetic field. In usual dispersive bands, the  $B$ -linear quantum correction is negligibly small in weak magnetic field limit compared to the zero-field band-width. This is the reason why the original Onsager's semiclassical scheme in Eq. (1) works well.

In the case of a flat band with zero band-width, on the other hand, the  $B$ -linear quantum correction always dominates the modified band structure  $E_{n,B}(\mathbf{k})$  in Eq. (3) even in weak magnetic field limit. Moreover, the modified band dispersion of an IFB is generally dispersive so that the relevant semiclassical orbits can be defined unambiguously. As a result, one can obtain the Landau levels of the IFB in the adjacent gapped regions by applying the semiclassical quantization rule to  $E_{n,B}(\mathbf{k})$ , which naturally explains the LLS of the IFB. The total magnitude  $\Delta$  of the LLS is determined by the difference between the maximum and the minimum values of  $E_{n,B}(\mathbf{k})$ , namely,  $\Delta = \max E_{n,B}(\mathbf{k}) - \min E_{n,B}(\mathbf{k})$ . This result is valid as long as the band gap  $E_{\text{gap}}$  between the IFB and its neighboring band at zero magnetic field is large enough, i.e.,  $E_{\text{gap}} \gg \max |E_{n,B}(\mathbf{k})|$ . The generic behavior of an IFB under magnetic field is schematically described in Figure 1 where one can clearly observe that the Landau levels of the IFB spread into the gaps at zero-field above

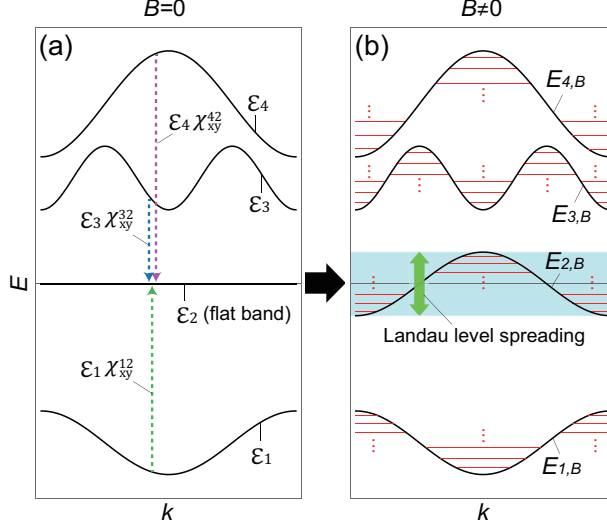


FIG. 1. **Landau level spreading (LLS) of an isolated flat band (IFB).** (a) The band structure of a 2D system in the absence of magnetic field. The second band with the energy  $\varepsilon_2 = 0$  corresponds to the IFB. The inter-band coupling  $\varepsilon_m \chi_{xy}^{m2}$  of the IFB with the other dispersive band of the energy  $\varepsilon_m$  ( $m = 1, 3, 4$ ) is indicated by a dashed vertical arrow. (b) The modified band dispersion  $E_{m,B}$  ( $m = 1, \dots, 4$ ) in the presence of the magnetic field. The corresponding Landau levels are shown by red solid lines. The LLS of the IFB is represented by the green arrow.

and below the IFB.

### Geometric interpretation: Fidelity tensor and cross-gap Berry connection

Interestingly, we find that the LLS of IFBs is a manifestation of the non-trivial wave function geometry of the flat band arising from inter-band couplings. One can show that the modified band dispersion of the IFB is given by

$$E_{n,B}(\mathbf{k}) = -2\pi \frac{\phi}{\phi_0} \frac{1}{A_0} \text{Im} \sum_{m \neq n} \varepsilon_m(\mathbf{k}) \chi_{xy}^{nm}(\mathbf{k}), \quad (5)$$

in which

$$\chi_{ij}^{nm}(\mathbf{k}) = \langle \partial_i u_n(\mathbf{k}) | u_m(\mathbf{k}) \rangle \langle u_m(\mathbf{k}) | \partial_j u_n(\mathbf{k}) \rangle = A_i^{nm}(\mathbf{k})^* A_j^{nm}(\mathbf{k}). \quad (6)$$

where  $\phi_0 = h/e$ ,  $\phi = BA_0$  is the magnetic flux per unit cell, and  $A_0$  is the unit cell area assumed to be  $A_0 = 1$ . Here, we assume that the  $n$ -th band is the IFB at the zero energy without loss of generality. We note that  $A_i^{nm}(\mathbf{k}) = \langle u_m(\mathbf{k}) | \partial_i u_n(\mathbf{k}) \rangle$  indicates the cross-gap Berry connection between the  $n$ -th and  $m$ -th bands ( $n \neq m$ ) defined above, and  $\chi_{ij}^{nm}(\mathbf{k})$  is the corresponding fidelity

tensor that describes the transition amplitude between the  $n$ -th and  $m$ -th bands as discussed below. Hence, Eq. (5) indicates that the modified band dispersion of the IFB is given by the summation of the transition amplitudes  $\chi_{xy}^{nm}(\mathbf{k})$  between the IFB and the  $m$ -th band weighted by the energy  $\varepsilon_m(\mathbf{k})$  of the  $m$ -th band as illustrated in Figure 1. This means that the immobile carriers with infinite effective mass in an IFB can respond to external magnetic field through the inter-band coupling, characterized by the cross-gap Berry connection, to dispersive bands. This clearly provides a new insight for understanding the Landau level structure of a flat band and its geometric character.

Let us discuss the geometric character of the fidelity tensor  $\chi_{xy}^{nm}(\mathbf{k})$  more explicitly. In general, the geometry of the quantum state  $u_n(\mathbf{k})$  can be derived from the Hilbert-Schmidt quantum distance [19–21] defined as

$$s(u_n(\mathbf{k}), u_n(\mathbf{k}')) = 1 - |\langle u_n(\mathbf{k}) | u_n(\mathbf{k}') \rangle|^2, \quad (7)$$

which measures the similarity between  $u_n(\mathbf{k})$  and  $u_n(\mathbf{k}')$ . For  $\mathbf{k}' = \mathbf{k} + d\mathbf{k}$ , we obtain

$$s(u_n(\mathbf{k}), u_n(\mathbf{k} + d\mathbf{k})) = \mathfrak{G}_{ij}^n(\mathbf{k}) dk_i dk_j, \quad (8)$$

where  $\mathfrak{G}_{ij}^n(\mathbf{k})$  indicates the quantum geometric tensor [22–24] whose explicit form is

$$\mathfrak{G}_{ij}^n(\mathbf{k}) = \sum_{m \neq n} \langle \partial_i u_n(\mathbf{k}) | u_m(\mathbf{k}) \rangle \langle u_m(\mathbf{k}) | \partial_j u_n(\mathbf{k}) \rangle = \sum_{m \neq n} \chi_{ij}^{nm}(\mathbf{k}), \quad (9)$$

which shows that the quantum geometric tensor  $\mathfrak{G}_{ij}^n(\mathbf{k})$  of the  $n$ -th band is given by the summation of the fidelity tensor  $\chi_{ij}^{nm}(\mathbf{k})$  over all  $m \neq n$ . We note that  $\chi_{ij}^{nm}(\mathbf{k})$  itself cannot define a distance as the triangle inequality is not satisfied. However, it is related to the transition probability or the fidelity  $F(u_n(\mathbf{k}), u_m(\mathbf{k}'))$  between the  $n$ -th and  $m$ -th bands [25] through the following relations:

$$F(u_n(\mathbf{k}), u_m(\mathbf{k}')) = |\langle u_n(\mathbf{k}) | u_m(\mathbf{k}') \rangle|^2, \quad (10)$$

$$F(u_n(\mathbf{k}), u_m(\mathbf{k} + d\mathbf{k})) = \chi_{ij}^{nm}(\mathbf{k}) dk_i dk_j. \quad (11)$$

Thus, the geometric interpretation based on Eqs. (5) and (11) clearly shows that the LLS originates from the inter-band coupling.

## Symmetry constraints on the LLS

The LLS of an IFB is strongly constrained by symmetry. First, we consider a generic symmetry  $\hat{\sigma}$  whose action on the Hamiltonian is given by

$$U_\sigma(\mathbf{k}) \overline{H(\mathbf{k})}^s U_\sigma(\mathbf{k})^\dagger = p H(O_\sigma \mathbf{k}), \quad (12)$$

where  $s \in \{0, 1\}$ ,  $p \in \{-1, 1\}$ , and  $U_\sigma(\mathbf{k})$  and  $O_\sigma$  are a unitary and orthogonal matrices representing  $\hat{\sigma}$ , respectively.  $\overline{x}^{s=1}$  denotes the complex conjugation of  $x$  while  $\overline{x}^{s=0} = x$ . Note that  $s = 0$  and  $1$  are relevant to the unitary and anti-unitary symmetries, respectively, while  $p = -1$  and  $+1$  correspond to anti-symmetry and symmetry, respectively.

Among all possible symmetries of the form in Eq. (12), we find that the modified band dispersion  $E_{n,B}(\mathbf{k})$  vanishes when the system respects the chiral  $C$  or space-time-inversion  $I_{ST}$  symmetries in the zero magnetic flux (see Methods and Supplementary Notes 1 and 2 for the detailed derivation).  $C$  and  $I_{ST}$  are characterized by  $(O_\sigma, s, p) = (\mathbb{1}, 0, -1)$  and  $(\mathbb{1}, 1, 1)$ , respectively, where  $\mathbb{1}$  is the identity matrix. In the following, we demonstrate that the LLS is proportional to  $B^2$  for a flat-band system with  $I_{ST}$  symmetry in the zero magnetic field, while the LLS is forbidden in the presence of chiral symmetry. Interestingly, although  $I_{ST}$  symmetry would be broken as the magnetic field is turned on, the LLS is strongly constrained by  $I_{ST}$  symmetry.

We further find that  $\max E_{n,B}(\mathbf{k}) = -\min E_{n,B}(\mathbf{k})$  when the system respects a symmetry satisfying  $(-1)^s p \text{Det} O_\sigma = -1$  and  $O_\sigma \neq \mathbb{1}$ , such as time-reversal  $T$  or reflection  $R$  symmetry, at the zero magnetic field (see Methods and Supplementary Note 1 for detailed derivations). This implies that the minimum and maximum values of the LLS have the same magnitude but with the opposite signs. The relevant tight-binding models are shown in the Supplementary Notes 3.

## Generic flat-band systems

We first consider the spin-orbit-coupled (SOC) Lieb model [26] as an example of generic flat-band systems. The lattice structure for this model is shown in Figure 2(a). The model consists of the nearest neighbor and the next nearest neighbor hoppings, which are denoted as green solid and dashed arrows, respectively, in Figure 2(a). The tight-binding Hamiltonian in momentum space is

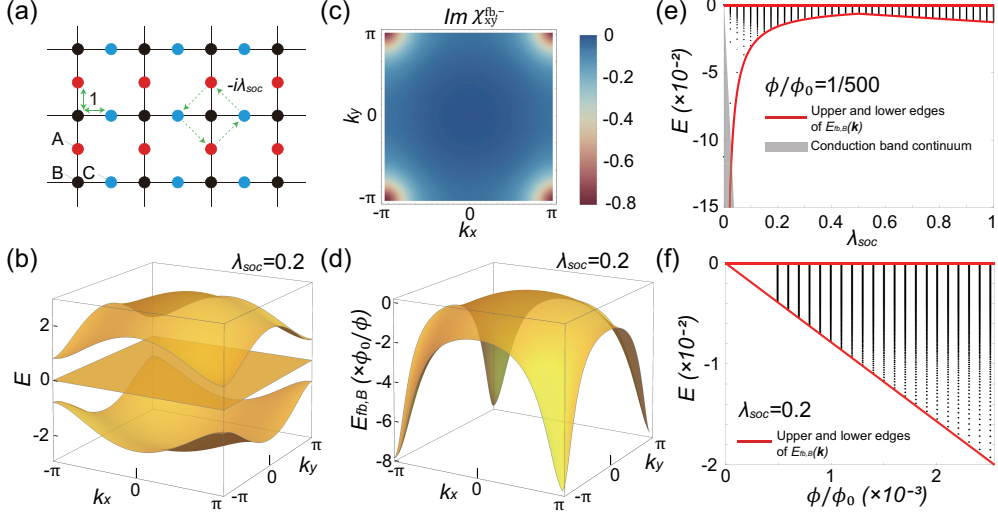


FIG. 2. **Landau level spreading of a generic system with an IFB.** (a) Lattice structure for the spin-orbit-coupled (SOC) Lieb model composed of three sublattices,  $A$ ,  $B$  and  $C$ . The double-headed green arrows denote the nearest neighbor hoppings, and the single-headed green arrows indicate the spin-orbit coupling between  $A$  and  $C$  sublattices. (b) The band structure of  $H_{\text{socL}}(\mathbf{k})$  with  $\lambda_{\text{soc}} = 0.2$ . (c) Distribution of  $\text{Im } \chi_{xy}^{\text{fb},-}(\mathbf{k})$ . Note that  $\text{Im } \chi_{xy}^{\text{fb},-}(\mathbf{k}) = -\text{Im } \chi_{xy}^{\text{fb},+}(\mathbf{k})$ . (d) The modified band dispersion  $E_{\text{fb},B}(\mathbf{k})$  of the flat band in the presence of magnetic flux. (e) Landau level spectra of the flat band (black dots) as a function of  $\lambda_{\text{soc}}$  for magnetic flux  $\phi/\phi_0 = 1/500$ . (f) Landau level spectra of the flat band (black dots) as a function of magnetic flux  $\phi/\phi_0$  for  $\lambda_{\text{soc}} = 0.2$ .

given by

$$H_{\text{socL}}(\mathbf{k}) = \begin{pmatrix} 0 & 2 \cos \frac{k_y}{2} & -4i\lambda_{\text{soc}} \sin \frac{k_x}{2} \sin \frac{k_y}{2} \\ 2 \cos \frac{k_y}{2} & 0 & 2 \cos \frac{k_x}{2} \\ 4i\lambda_{\text{soc}} \sin \frac{k_x}{2} \sin \frac{k_y}{2} & 2 \cos \frac{k_x}{2} & 0 \end{pmatrix}, \quad (13)$$

where  $\lambda_{\text{soc}}$  denotes the strength of spin-orbit coupling. The flat band's energy is zero, i.e.,  $\varepsilon_{\text{socL,fb}}(\mathbf{k}) = 0$ , and the energies of the other two bands are

$$\varepsilon_{\text{socL},\pm}(\mathbf{k}) = \pm 2 \sqrt{\cos^2 \frac{k_x}{2} + \cos^2 \frac{k_y}{2} + 4\lambda_{\text{soc}}^2 \sin^2 \frac{k_x}{2} \sin^2 \frac{k_y}{2}}, \quad (14)$$

which are plotted in Figure 2(b) for  $\lambda_{\text{soc}} = 0.2$ . The band gap between the IFB and its neighboring bands is given by  $4|\lambda_{\text{soc}}|$  if  $|\lambda_{\text{soc}}| < 1/2$ , and 2 if  $|\lambda_{\text{soc}}| \geq 1/2$ , thus the flat band is decoupled from other bands for non-zero  $\lambda_{\text{soc}}$ .

The analytic form of the fidelity tensor  $\chi_{xy}^{nm}(\mathbf{k})$  is given by

$$\chi_{\text{socL},xy}^{\text{fb},+}(\mathbf{k}) = \left( \chi_{\text{socL},xy}^{\text{fb},-}(\mathbf{k}) \right)^* = \frac{f(k_x, k_y) f(k_y, k_x)}{(\varepsilon_{\text{socL},+}(\mathbf{k}))^4 (2 + \cos k_x + \cos k_y)}, \quad (15)$$

where  $f(k_x, k_y) = 4\lambda_{\text{soc}} \sin \frac{k_x}{2} \cos \frac{k_y}{2} (\cos^2 \frac{k_x}{2} + 1) + i\varepsilon_{\text{socL},+}(\mathbf{k}) \cos \frac{k_x}{2} \sin \frac{k_y}{2}$ . Then, from (5), the modified band dispersion for the flat band is given by

$$E_{\text{fb},B}^{\text{socL}}(\mathbf{k}) = -\frac{2\pi\lambda_{\text{soc}} (3 - \cos k_x - \cos k_y - \cos k_x \cos k_y)}{(\varepsilon_{\text{socL},+}(\mathbf{k}))^2} \frac{\phi}{\phi_0}. \quad (16)$$

In Figures 2(c) and (d),  $\text{Im} \chi_{xy}^{\text{fb},-}(\mathbf{k})$  and  $E_{\text{fb},B}(\mathbf{k})$  are shown. We note that

$$\max E_{\text{fb},B}^{\text{socL}}(\mathbf{k}) = E_{\text{fb},B}^{\text{socL}}(0, 0) = 0, \quad (17)$$

$$\min E_{\text{fb},B}^{\text{socL}}(\mathbf{k}) = \begin{cases} E_{\text{fb},B}^{\text{socL}}(\pi, \pi) = -\frac{\pi}{2\lambda_{\text{soc}}} \frac{\phi}{\phi_0} & (\lambda_{\text{soc}} \leq \frac{1}{2}) \\ E_{\text{fb},B}^{\text{socL}}(0, \pi) = -2\pi\lambda_{\text{soc}} \frac{\phi}{\phi_0} & (\lambda_{\text{soc}} > \frac{1}{2}) \end{cases}. \quad (18)$$

These minimum and maximum values of  $E_{\text{fb},B}^{\text{socL}}(\mathbf{k})$  correspond to the lower and upper bounds for the LLS of the IFB as illustrated by red lines in Figures 2(e) and (f). Interestingly, the fidelity tensors  $\chi_{\text{socL},xy}^{\text{fb},+}(\mathbf{k})$  and  $\chi_{\text{socL},xy}^{\text{fb},-}(\mathbf{k})$  are conjugate of each other. This originates from the anti-unitary symmetry  $C \circ I_{ST}$ , a combination of chiral  $C$  and space-time-inversion  $I_{ST}$  symmetries, present in the system (see Supplementary Note 1 for the details.)

## Chiral-symmetric system

We construct a chiral-symmetric Lieb (c-Lieb) model as a representative example for chiral-symmetric IFB systems. The c-Lieb is defined on the same Lieb lattice as the SOC-Lieb model, but with different hoppings. As shown in Figure 3(a), this model consists only of the nearest neighbor hoppings, denoted by green arrows. The hopping parameter from a B-site to a C-site is  $t_1$  for the rightward hopping, and 1 for the leftward hopping. On the other hand, the hopping parameter from a B-site to an A-site is  $t_2$  for the upward hopping, and 1 for the downward hopping. The

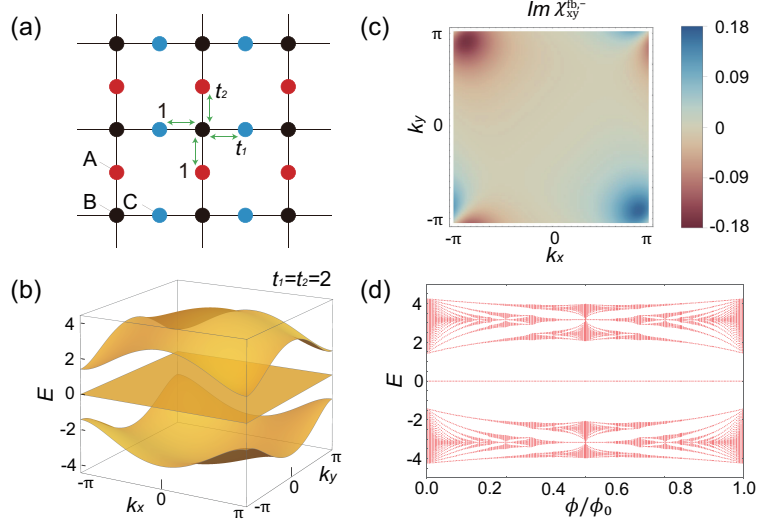


FIG. 3. **Landau level spreading of a flat-band system with chiral symmetry.** (a) Lattice structure for the c-Lieb model. The green arrows denote the hoppings. Note that the direction dependent hopping parameters induce a finite gap between the flat band and other bands. (b) The band structure for  $H_{\text{cL}}(\mathbf{k})$  with  $t_1 = t_2 = 2$ . (c) Distribution of  $\text{Im } \chi_{xy}^{\text{fb},-}(\mathbf{k})$ . Due to the chiral symmetry,  $\text{Im } \chi_{xy}^{\text{fb},-}(\mathbf{k}) = \text{Im } \chi_{xy}^{\text{fb},+}(\mathbf{k})$  holds. (d) The Hofstadter spectrum of the c-Lieb model  $H_{\text{cL}}(\mathbf{k})$  with  $t_1 = t_2 = 2$ . For any value of magnetic flux, the Landau levels of the flat band are fixed to the zero energy.

corresponding tight-binding Hamiltonian in momentum space is given by

$$H_{\text{cL}}(\mathbf{k}) = \begin{pmatrix} 0 & e^{i\frac{k_y}{2}} + t_2 e^{-i\frac{k_y}{2}} & 0 \\ e^{-i\frac{k_y}{2}} + t_2 e^{i\frac{k_y}{2}} & 0 & e^{-i\frac{k_x}{2}} + t_1 e^{i\frac{k_x}{2}} \\ 0 & e^{i\frac{k_x}{2}} + t_1 e^{-i\frac{k_x}{2}} & 0 \end{pmatrix}. \quad (19)$$

with energy eigenvalues  $\varepsilon_{\text{cL,fb}}(\mathbf{k}) = 0$  and  $\varepsilon_{\text{cL,}\pm}(\mathbf{k}) = \pm\sqrt{2 + t_1^2 + t_2^2 + 2t_1 \cos k_x + 2t_2 \cos k_y}$ . The chiral symmetry operator  $C$  is given by  $C = \text{Diag}(1, -1, 1)$  which gives a symmetry relation,

$$CH_{\text{cL}}(\mathbf{k})C^{-1} = -H_{\text{cL}}(\mathbf{k}). \quad (20)$$

Note that the wave function of the flat band is also a simultaneous eigenstate of the chiral symmetry having a definite chiral charge  $c = +1$ :

$$C|u_{\text{cL,fb}}(\mathbf{k})\rangle = c|u_{\text{cL,fb}}(\mathbf{k})\rangle. \quad (21)$$

Also, we obtain the fidelity tensor  $\chi_{xy}^{\text{fb},\pm}$ , expressed by

$$\chi_{\text{cL},xy}^{\text{fb},+}(\mathbf{k}) = \chi_{\text{cL},xy}^{\text{fb},-}(\mathbf{k}) = -\frac{(1+t_1e^{ik_x})(1-t_1e^{-ik_x})(1+t_2e^{-ik_y})(1-t_2e^{ik_y})}{8(\varepsilon_{\text{cL},+}(\mathbf{k}))^4}. \quad (22)$$

The band structure and  $\chi_{\text{cL},xy}^{\text{fb},-}(\mathbf{k})$  are shown in Figures 3(b) and (c). Eq. (22) indicates that the modified band dispersion  $E_{\text{fb},B}(\mathbf{k})$  vanishes for all  $\mathbf{k}$  because  $\varepsilon_{\text{cL},+}(\mathbf{k}) = -\varepsilon_{\text{cL},-}(\mathbf{k})$ , which means that there is no LLS in the weak magnetic field. Also, we calculate the Hofstadter spectrum for the c-Lieb model. Interestingly, we find that the LLS is absent even in the strong magnetic field, as shown in Figure 3(d). The existence of such zero-energy flat bands in the finite magnetic flux is guaranteed by chiral symmetry  $C$ . As explained in Supplementary Note 2, the minimal number of zero-energy flat bands is given by  $|\text{Tr}[C]|$  at the zero magnetic flux. Moreover, when the system has the  $|\text{Tr}[C]|(>0)$  number of zero-energy flat bands at the zero magnetic flux, the LLS of flat band(s) is forbidden unless a gap closes at  $E = 0$  as the magnetic flux increases (see Supplementary Note 2). In the c-Lieb model, such a gap closing at  $E = 0$  does not occur at any magnetic flux. Hence, there is no LLS in all range of magnetic flux. On the other hand, when a gap closes at  $E = 0$  as the magnetic flux increases, the LLS is forbidden only in a finite range of magnetic flux. As an example, in Supplementary Note 3, we show the Hofstadter spectrum of the ten-band model for twisted-bilayer graphene proposed in Ref. 27.

### Space-time-inversion-symmetric system

The LLS of an IFB is weakly dependent on magnetic field when the system respects space-time-inversion  $I_{ST}$  symmetry at zero magnetic field. We consider spinless fermions on the checkerboard lattice shown in Figure 4(a), which is sometimes called the Tasaki or decorated square lattice [28–30]. This model respects both time-reversal  $T$  and inversion  $I$  symmetries. Hence, a combined symmetry, space-time-inversion symmetry  $I_{ST} = I \circ T$ , exists. We note that the following discussion holds even if  $T$  and  $I$  are broken as long as  $I_{ST}$  is not broken. The tight-binding Hamiltonian consists of the hopping processes up to the third nearest neighbor hopping. In momentum space,

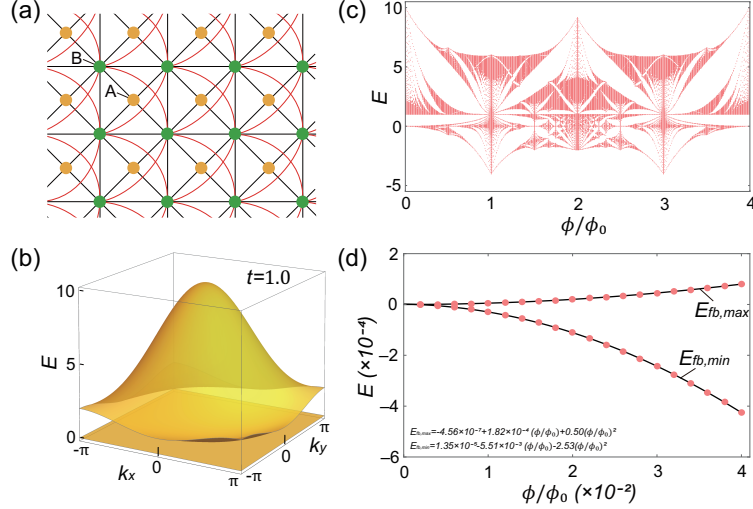


FIG. 4. **Landau level spreading of a flat-band system with space-time-inversion symmetry.** (a) The lattice structure for the  $I_{ST}$ -symmetric checkerboard model. The red and black lines denote the hopping processes between  $A$  and  $B$  sublattices. (b) The band structure of  $H_{I_{ST}}(\mathbf{k})$  with  $t = 1.0$ . (c) The Hofstadter spectrum of the  $I_{ST}$ -symmetric checkerboard model with  $t = 1.0$ . (d) Variation of the lowest and highest Landau levels related to the flat band in the weak magnetic field.  $E_{fb,min}$  and  $E_{fb,max}$  indicate the corresponding fitting functions that exhibit quadratic magnetic field dependence dominantly.

the Hamiltonian is written as

$$H_{I_{ST}}(\mathbf{k}) = \begin{pmatrix} 1 & \cos \frac{k_+}{2} + 2t \cos \frac{k_-}{2} \\ \cos \frac{k_+}{2} + 2t \cos \frac{k_-}{2} & 2t \cos k_x + 2t \cos k_y + \cos^2 \frac{k_+}{2} + 4t^2 \cos^2 \frac{k_-}{2} \end{pmatrix}, \quad (23)$$

$$= \begin{pmatrix} 1 \\ \cos \frac{k_+}{2} + 2t \cos \frac{k_-}{2} \end{pmatrix} \left( 1 \cos \frac{k_+}{2} + 2t \cos \frac{k_-}{2} \right), \quad (24)$$

where  $k_{\pm} = k_x \pm k_y$ . For  $t = 1.0$ , the band structure is shown in Figure 4(b). This system hosts a flat band with zero energy and a dispersive band with positive energy. The energy eigenvalues are given by  $\varepsilon_{I_{ST},\uparrow}(\mathbf{k}) = 1 + (\cos \frac{k_+}{2} + 2t \cos \frac{k_-}{2})^2$  and  $\varepsilon_{I_{ST},fb}(\mathbf{k}) = 0$ .

In this system,  $I_{ST}$  is simply given by the complex conjugation, i.e.,  $I_{ST} = \mathcal{K}$  and

$$I_{ST}|u_{I_{ST},fb/\uparrow}(\mathbf{k})\rangle = |u_{I_{ST},fb/\uparrow}(\mathbf{k})\rangle. \quad (25)$$

Also, explicit calculations show  $\text{Im } \chi_{I_{ST},xy}^{\text{fb},\uparrow}(\mathbf{k}) = 0$  and  $E_{n,B}(\mathbf{k}) = 0$ , which results from Eq. (25).

In Supplementary Note 1, we have proved that space-time inversion  $I_{ST}$  imposes  $E_{n,B}(\mathbf{k}) = 0$

in general. We also note that  $E_{n,B}(\mathbf{k}) = 0$  is consistent with the fact that the orbital angular momentum, which is proportional to the orbital magnetic moment  $\mu$ , is constrained to be zero in  $I_{ST}$ -symmetric systems. Although the LLS is negligible in the weak magnetic field, it becomes considerably large in the strong magnetic field as shown in the Hofstadter spectrum in Figure 4(c). As shown in Figure 4(c), the Landau levels of the flat band acquire or lose their energy as the magnetic flux increases from 0 to some finite value much less than 1. This implies that the higher-order corrections of the magnetic field must be considered. Although it is out of the scope of this work, we present a fitting of the highest and lowest Landau levels of the flat band with respect to the magnetic flux:

$$E_{\text{fb,min}}\left(\frac{\phi}{\phi_0}\right) = 1.35 \times 10^{-5} - 5.51 \times 10^{-3} \left(\frac{\phi}{\phi_0}\right) - 2.53 \left(\frac{\phi}{\phi_0}\right)^2, \quad (26)$$

$$E_{\text{fb,max}}\left(\frac{\phi}{\phi_0}\right) = -4.56 \times 10^{-7} + 1.82 \times 10^{-4} \left(\frac{\phi}{\phi_0}\right) + 0.50 \left(\frac{\phi}{\phi_0}\right)^2, \quad (27)$$

which is plotted in Figure 4(d) where one can observe the dominant quadratic dependence on the magnetic field.

Finally, we comment on the gap closing at  $(\phi/\phi_0, E) = (1, 1.0)$  in the Hofstadter spectrum in Figure 4(c). At  $(\phi/\phi_0, E) = (1, 1.0)$ , the Landau levels related to the flat and dispersive bands show a closing of an indirect gap. We note that there is no closing of direct gaps in the Hofstadter Hamiltonian. Unlike the inevitable closing of the direct gap between topological bands in the finite magnetic flux reported before [11, 31], it is not necessary to close a direct gap in our system.

## Discussion

We have shown that the LLS of an IFB is determined by its wave function geometry and the underlying symmetry of the system. The idea presented in this work goes far beyond the conventional semiclassical idea in which the Landau level spectrum is dominantly determined by the band dispersion at zero magnetic field. So far, we have focused on the cases when the band width of the IFB is strictly zero. However, in real materials, it is difficult to observe perfect flat bands due to the long-range hoppings and spin-orbit coupling [32–36]. To understand the influence of a finite band width of the IFB, we have studied another tight-binding model defined in the Lieb lattice including spin-orbit coupling. The hopping parameters, the band structure, and the LLS of this system are described in Figures 5(a), (b), and (c)-(d), respectively. Under weak magnetic flux with  $t\phi > 0$ , the

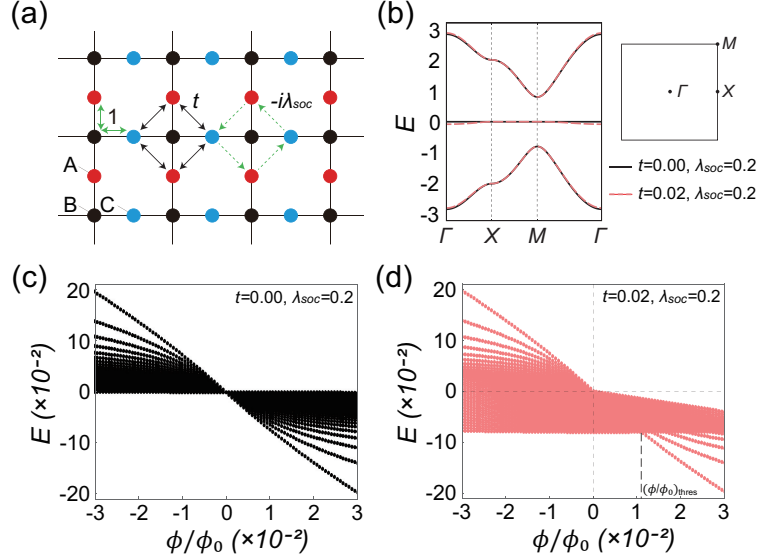


**FIG. 5. Landau level spreading of a nearly-flat-band system** (a) Lattice structure for the nearly-flat-Lieb model. The next nearest hoppings from  $A$  to  $C$  with strength  $t$  are considered additionally, compared with the spin-orbit-coupled Lieb model. (b) The band structure of the nearly-flat-Lieb model with  $(t, \lambda_{soc}) = (0.00, 0.2)$  and  $(0.02, 0.2)$ , which are denoted by the black and red lines, respectively. The right side of band structure defines the Brillouin zone and the high-symmetry points. (c) The Landau levels in the weak magnetic field for  $t = 0.00$  and  $\lambda_{soc} = 0.2$ . The lowest (highest) Landau level has the energy  $-\frac{\pi}{2\lambda_{soc}}\frac{\phi}{\phi_0}$  when  $t\phi > 0$  ( $t\phi < 0$ ). Since the band width of a flat band is zero in the absence of magnetic field, the LLS can be clearly observed. (d) Similar to (c) but for  $t = 0.02$  and  $\lambda_{soc} = 0.2$ . When  $t\phi > 0$ , the LLS can be observed once the magnetic flux exceeds the threshold value  $(\phi/\phi_0)_{\text{thres}} \sim \frac{8t\lambda_{soc}}{\pi}$  because of the finite band width  $4t$ . While, a threshold magnetic flux for observing the LLS is zero when  $t\phi < 0$  since the LLS develops only in the negative energy direction and the band width does not screen the LLS.

LLS of the IFB cannot be observed because it is dominated by the energy scale of the band width of the nearly flat band. However, the anomalous LLS arising from the wave function geometry can be observed for the magnetic flux larger than a threshold value  $(\phi/\phi_0)_{\text{thres}} \sim 8t\lambda_{soc}/\pi$ . On the other hand, the LLS is not disturbed by the band width when  $t\phi < 0$ , because the nearly flat band has only positive energy. Such a Lieb lattice model with spin-orbit coupling hosting a nearly flat band was already realized in an exciton-polariton system [37], and also is expected to be realized in electronic systems consisting of covalently-bonded organic frameworks [38].

## Method

**Symmetry constraints on the LLS.** In order to derive the symmetry constraints on  $E_{n,B}(\mathbf{k})$  and

$\chi_{xy}^{nm}(\mathbf{k})$ , let us consider a symmetry operation  $\hat{\sigma}$  acting on the Hamiltonian,

$$U_\sigma(\mathbf{k}) \overline{H(\mathbf{k})}^s U_\sigma(\mathbf{k})^\dagger = p H(O_\sigma \mathbf{k}), \quad (28)$$

where  $s \in \{0, 1\}$ ,  $p \in \{-1, 1\}$ ,  $U_\sigma$  indicates a unitary matrix representing the symmetry  $\hat{\sigma}$ , and  $\overline{x} = x^*$  means the complex conjugation of  $x$ . From now on, we use a compact notation  $\mathbf{g}_\sigma = (O_\sigma, s, p)$  to describe the operation of the symmetry  $\hat{\sigma}$ . For example,  $\mathbf{g}_T = (-\mathbb{1}_d, 1, 1)$  is used for time-reversal symmetry  $T$  where  $d$  and  $\mathbb{1}_d$  denote the dimensionality and the  $d \times d$  identity matrix, respectively. The symmetry constraints on  $E_{n,B}(\mathbf{k})$  and  $\chi_{ij}^{nm}(\mathbf{k})$  derived from Eq. (28) are

$$E_{n,B}(O_\sigma \mathbf{k}) = (-1)^s p \text{Det} O_\sigma E_{n,B}(\mathbf{k}), \quad (29)$$

$$\chi_{ij}^{nm\sigma}(O_\sigma \mathbf{k}) = [O_\sigma]_{ii'} [O_\sigma]_{jj'} \overline{\chi_{i'j'}^{nm}(\mathbf{k})}^s, \quad (30)$$

where the band indices  $m$  and  $m_\sigma$  in Eq. (30) are chosen such that  $\varepsilon_m(\mathbf{k}) = p \varepsilon_{m_\sigma}(O_\sigma \mathbf{k})$ . Detailed derivation of Eqs. (29) and (30) and comments on the degenerate bands can be found in Supplementary Note 1. From Eq. (29), we obtain two symmetries that give vanishing modified band dispersion,  $E_{n,B}(\mathbf{k}) = 0$ :  $\mathbf{g}_C = (\mathbb{1}_d, 0, -1)$  and  $\mathbf{g}_{I_{ST}} = (\mathbb{1}_d, 1, 1)$  which correspond to chiral symmetry  $C$  and space-time-inversion symmetry  $I_{ST}$ , respectively. On the other hand, when  $(-1)^s p \text{Det} O_\sigma = -1$  and  $\text{Det} O_\sigma \neq \mathbb{1}$ , the modified band dispersion satisfies  $E_{n,B}(O_\sigma \mathbf{k}) = -E_{n,B}(\mathbf{k})$ , which implies  $\max E_{n,B}(\mathbf{k}) = -\min E_{n,B}(\mathbf{k})$ . Time-reversal  $T$  and reflection  $R$  symmetries belong to this case. Also, the contribution to the  $E_{n,B}(\mathbf{k})$  from each band via the inter-band coupling in Eq. (5) can be systematically understood by using Eq. (30) (see Supplementary Note 1 for details).

**Calculation scheme for the Landau levels** We calculate the Hofstadter spectrum by numerically implementing the Peierls substitution to the tight-binding Hamiltonian.

## References

- [1] Onsager, L. Interpretation of the de Haas-van Alphen effect. *The London, Edinburgh, and Dublin Philosophical Magazine and Journal of Science* **43**, 1006–1008 (1952).
- [2] Roth, L. M. Semiclassical theory of magnetic energy levels and magnetic susceptibility of Bloch

electrons. *Physical Review* **145**, 434 (1966).

[3] Mikitik, G. & Sharlai, Y. V. Manifestation of Berry's phase in metal physics. *Physical Review Letters* **82**, 2147 (1999).

[4] Gao, Y. & Niu, Q. Zero-field magnetic response functions in Landau levels. *Proceedings of the National Academy of Sciences* **114**, 7295–7300 (2017).

[5] Fuchs, J.-N., Piéchon, F. & Montambaux, G. Landau levels, response functions and magnetic oscillations from a generalized Onsager relation. *SciPost Physics* **4**, 024 (2018).

[6] Zhang, Y., Tan, Y.-W., Stormer, H. L. & Kim, P. Experimental observation of the quantum Hall effect and Berry's phase in graphene. *Nature* **438**, 201–204 (2005).

[7] Novoselov, K. S. et al. Unconventional quantum Hall effect and Berry's phase of  $2\pi$  in bilayer graphene. *Nature Physics* **2**, 177–180 (2006).

[8] Chang, M.-C. & Niu, Q. Berry phase, hyperorbits, and the Hofstadter spectrum: Semiclassical dynamics in magnetic Bloch bands. *Physical Review B* **53**, 7010 (1996).

[9] Po, H. C., Watanabe, H. & Vishwanath, A. Fragile topology and Wannier obstructions. *Physical Review Letters* **121**, 126402 (2018).

[10] Ahn, J., Park, S. & Yang, B.-J. Failure of Nielsen-Ninomiya theorem and fragile topology in two-dimensional systems with space-time inversion symmetry: application to twisted bilayer graphene at magic angle. *Physical Review X* **9**, 021013 (2019).

[11] Lian, B., Xie, F. & Bernevig, B. A. Landau level of fragile topology. *Physical Review B* **102**, 041402 (2020).

[12] Rhim, J.-W. & Yang, B.-J. Classification of flat bands according to the band-crossing singularity of Bloch wave functions. *Physical Review B* **99**, 045107 (2019).

[13] Ma, J. et al. Direct observation of flatband loop states arising from nontrivial real-space topology. *Physical Review Letters* **124**, 183901 (2020).

[14] Rhim, J.-W., Kim, K. & Yang, B.-J. Quantum distance and anomalous Landau levels of flat bands. *Nature* **584**, 59–63 (2020).

[15] Chen, L., Mazaheri, T., Seidel, A. & Tang, X. The impossibility of exactly flat non-trivial Chern bands in strictly local periodic tight binding models. *Journal of Physics A: Mathematical and Theoretical* **47**, 152001 (2014).

[16] Read, N. Compactly supported Wannier functions and algebraic K-theory. *Physical Review B* **95**, 115309 (2017).

[17] Alexandradinata, A. & Höller, J. No-go theorem for topological insulators and high-throughput identification of Chern insulators. *Physical Review B* **98**, 184305 (2018).

[18] de Juan, F., Grushin, A. G., Morimoto, T. & Moore, J. E. Quantized circular photogalvanic effect in Weyl semimetals. *Nature Communications* **8**, 1–7 (2017).

[19] Bužek, V. & Hillery, M. Quantum copying: Beyond the no-cloning theorem. *Physical Review A* **54**, 1844 (1996).

[20] Dodonov, V., Man'Ko, O., Man'Ko, V. & Wünsche, A. Hilbert-Schmidt distance and non-classicality of states in quantum optics. *Journal of Modern Optics* **47**, 633–654 (2000).

[21] Berry, M. V. The quantum phase, five years after. *Geometric phases in physics* 7–28 (1989).

[22] Provost, J. & Vallee, G. Riemannian structure on manifolds of quantum states. *Communications in Mathematical Physics* **76**, 289–301 (1980).

[23] Zanardi, P., Giorda, P. & Cozzini, M. Information-theoretic differential geometry of quantum phase transitions. *Physical Review Letters* **99**, 100603 (2007).

[24] Ma, Y.-Q., Chen, S., Fan, H., Liu, W.-M. *et al.* Abelian and non-Abelian quantum geometric tensor. *Physical Review B* **81**, 245129 (2010).

[25] Jozsa, R. Fidelity for mixed quantum states. *Journal of modern optics* **41**, 2315–2323 (1994).

[26] Goldman, N., Urban, D. & Bercioux, D. Topological phases for fermionic cold atoms on the Lieb lattice. *Physical Review A* **83**, 063601 (2011).

[27] Po, H. C., Zou, L., Senthil, T. & Vishwanath, A. Faithful tight-binding models and fragile topology of magic-angle bilayer graphene. *Physical Review B* **99**, 195455 (2019).

[28] Tasaki, H. Ferromagnetism in the Hubbard models with degenerate single-electron ground states. *Physical Review Letters* **69**, 1608 (1992).

[29] Aoki, H., Ando, M. & Matsumura, H. Hofstadter butterflies for flat bands. *Physical Review B* **54**, R17296 (1996).

[30] Misumi, T. & Aoki, H. New class of flat-band models on tetragonal and hexagonal lattices: Gapped versus crossing flat bands. *Physical Review B* **96**, 155137 (2017).

[31] Herzog-Arbeitman, J., Song, Z.-D., Regnault, N. & Bernevig, B. A. Hofstadter topology: Non-crystalline topological materials in the Moiré era. *arXiv preprint arXiv:2006.13938* (2020). URL <https://arxiv.org/abs/2006.13938>.

[32] Taie, S. *et al.* Coherent driving and freezing of bosonic matter wave in an optical Lieb lattice. *Science Advances* **1**, e1500854 (2015).

- [33] Kajiwara, S., Urade, Y., Nakata, Y., Nakanishi, T. & Kitano, M. Observation of a nonradiative flat band for spoof surface plasmons in a metallic Lieb lattice. *Physical Review B* **93**, 075126 (2016).
- [34] Slot, M. R. *et al.* Experimental realization and characterization of an electronic Lieb lattice. *Nature Physics* **13**, 672–676 (2017).
- [35] Drost, R., Ojanen, T., Harju, A. & Liljeroth, P. Topological states in engineered atomic lattices. *Nature Physics* **13**, 668–671 (2017).
- [36] Leykam, D., Andrianov, A. & Flach, S. Artificial flat band systems: from lattice models to experiments. *Advances in Physics: X* **3**, 1473052 (2018).
- [37] Whittaker, C. *et al.* Exciton polaritons in a two-dimensional Lieb lattice with spin-orbit coupling. *Physical Review Letters* **120**, 097401 (2018).
- [38] Cui, B. *et al.* Realization of Lieb lattice in covalent-organic frameworks with tunable topology and magnetism. *Nature Communications* **11**, 1–8 (2020).
- [39] Song, Z. *et al.* All magic angles in twisted bilayer graphene are topological. *Physical Review Letters* **123**, 036401 (2019).

## Acknowledgments

Y.H. was supported by IBS-R009-D1 and Samsung Science and Technology Foundation under Project Number SSTF-BA2002-06. J.W.R. was supported by IBS-R009-D1. B.J.Y. was supported by the Institute for Basic Science in Korea (Grant No. IBS-R009-D1), Samsung Science and Technology Foundation under Project Number SSTF-BA2002-06, Basic Science Research Program through the National Research Foundation of Korea (NRF) (Grant No. 0426-20200003), and the US Army Research Office under Grant No. W911NF-18-1-0137.

## Author contributions

All authors contributed equally to all aspects of the paper.

## Additional information

**Competing interests:** The authors declare no competing interests.

**Materials & Correspondence:** should be addressed to J.-W. R. or B.-J. Y.



## Supplementary Information

### Supplementary Note 1. Symmetry constraint on the Landau level spreading of flat band

In this section, we study the symmetry transformation of the modified band dispersion  $E_{n,B}(\mathbf{k})$  and the fidelity tensor  $\chi_{ij}^{nm}(\mathbf{k})$ . Here, we use a compact notation which can be applied to both unitary and anti-unitary (anti)-symmetries. In this notation, any symmetry operation  $\hat{\sigma}$  can be expressed by

$$U_\sigma(\mathbf{k}) \overline{H(\mathbf{k})}^s U_\sigma(\mathbf{k})^\dagger = p H(O_\sigma \mathbf{k}), \quad (\text{S1})$$

$$\mathbf{g}_\sigma = (O_\sigma, s, p), \quad (\text{S2})$$

where  $s = 0, 1$  and  $p = \pm 1$ . The bar notation denotes the complex conjugation, i.e.,  $\bar{x} = x^*$ . For example,  $\mathbf{g}_\sigma = (\mathbb{1}, 0, -1)$  and  $(-\mathbb{1}, 1, 1)$  correspond to chiral and time-reversal symmetries, respectively, where  $\mathbb{1}$  denotes the identity matrix. First consequence of symmetry in Eq. (S2) is that the band structure is symmetric with respect to  $\sigma$ . Namely,  $p \varepsilon(\mathbf{k})$  is the corresponding energy eigenvalue at  $O_\sigma \mathbf{k}$  for an energy eigenvalue  $\varepsilon(\mathbf{k})$  in the band structure. Furthermore, symmetry relations are imposed on the energy eigenstates as follows.

$$U_\sigma(\mathbf{k}) \overline{|u_m(\mathbf{k})\rangle}^s = |u_{m_\sigma}(O_\sigma \mathbf{k})\rangle B_\sigma(\mathbf{k})_{m_\sigma m} \quad (m \neq n), \quad (\text{S3})$$

$$U_\sigma(\mathbf{k}) \overline{|u_n(\mathbf{k})\rangle}^s = |u_n(O_\sigma \mathbf{k})\rangle e^{i\phi_n(\mathbf{k})}, \quad (\text{S4})$$

for dispersive bands  $m$  ( $m \neq n$ ) and the flat band  $n$ , respectively. Here, the band indices are defined such that  $\varepsilon_m(\mathbf{k}) = p \varepsilon_{m_\sigma}(O_\sigma \mathbf{k})$ , and  $B_\sigma(\mathbf{k})_{m_\sigma m}$  and  $e^{i\phi_n(\mathbf{k})}$  are unitary and periodic in the Brillouin zone. With the symmetry transformation of energy eigenstates defined above in Eqs. (S3) and (S4), one can derive symmetry constraint on the modified band dispersion  $E_{n,B}(\mathbf{k})$  and the fidelity tensor  $\chi_{ij}^{nm}(\mathbf{k})$ .

### Symmetry constraint on the modified band dispersion $E_{n,B}(\mathbf{k})$

We recall the definition of modified band dispersion  $E_{n,B}(\mathbf{k})$ :

$$E_{n,B}(\mathbf{k}) = -2\pi \frac{\phi}{\phi_0} \frac{1}{A_0} \text{Im} \langle \partial_x u_n(\mathbf{k}) | H(\mathbf{k}) | \partial_y u_n(\mathbf{k}) \rangle. \quad (\text{S5})$$

Note that  $n$ -th band is an isolated flat band with  $\varepsilon_n(\mathbf{k}) = 0$ . Now, we study the symmetry transformation of  $l_{ij}^n(\mathbf{k}) := \langle \partial_i u_n(\mathbf{k}) | H(\mathbf{k}) | \partial_j u_n(\mathbf{k}) \rangle$  by using Eq. (S4):

$$\begin{aligned}
l_{ij}^n(O_\sigma \mathbf{k}) &= \left[ \langle \partial_{\mathbf{k}'_i} u_n(\mathbf{k}') | H(\mathbf{k}') | \partial_{\mathbf{k}'_j} u_n(\mathbf{k}') \rangle \right]_{\mathbf{k}'=O_\sigma \mathbf{k}} \\
&= [O_\sigma]_{ii'} [O_\sigma]_{jj'} \partial_{i'} \left( e^{i\phi_n(\mathbf{k})} \overline{\langle u_n(\mathbf{k}) \rangle}^s U_\sigma(\mathbf{k})^\dagger \right) \\
&\quad \times \left( p U_\sigma(\mathbf{k}) \overline{H(\mathbf{k})}^s U_\sigma(\mathbf{k})^\dagger \right) \partial_{j'} \left( e^{-i\phi_n(\mathbf{k})} U_\sigma(\mathbf{k}) \overline{\langle u_n(\mathbf{k}) \rangle}^s \right) \\
&= p [O_\sigma]_{ii'} [O_\sigma]_{jj'} \overline{\langle \partial_{i'} u_n(\mathbf{k}) | H(\mathbf{k}) | \partial_{j'} u_n(\mathbf{k}) \rangle}^s \\
&= p [O_\sigma]_{ii'} [O_\sigma]_{jj'} \overline{l_{i'j'}^n(\mathbf{k})}^s.
\end{aligned} \tag{S6}$$

Hence, we obtain

$$\begin{aligned}
E_{n,B}(O_\sigma \mathbf{k}) &= -2\pi \frac{\phi}{\phi_0} \frac{1}{A_0} \text{Im} \left[ p [O_\sigma]_{xi} [O_\sigma]_{yj} \overline{l_{ij}^n(\mathbf{k})}^s \right] \\
&= -(-1)^s p ([O_\sigma]_{xx} [O_\sigma]_{yy} - [O_\sigma]_{xy} [O_\sigma]_{yx}) \times 2\pi \frac{\phi}{\phi_0} \frac{1}{A_0} \text{Im} l_{xy}^n(\mathbf{k}) \\
&= (-1)^s p \text{Det} O_\sigma E_{n,B}(\mathbf{k}).
\end{aligned} \tag{S7}$$

Note that  $l_{xx}^n(\mathbf{k})$  and  $l_{yy}^n(\mathbf{k})$  are real, thus  $\text{Im} l_{xx}^n(\mathbf{k}) = \text{Im} l_{yy}^n(\mathbf{k}) = 0$ . We remark two cases when the LLS is strongly constrained by symmetry. First, when  $(-1)^s p = -1$  and  $O_\sigma = \mathbb{1}$  are satisfied at the same time, the modified band dispersion  $E_{n,B}(\mathbf{k}) = 0$  vanishes. Chiral symmetry  $C$  and space-time-inversion symmetry  $I_{ST}$ , characterized by  $\mathbf{g}_C = (\mathbb{1}, 0, -1)$  and  $\mathbf{g}_{I_{ST}} = (\mathbb{1}, 1, 1)$  respectively, belong to this case. The second case is when  $(-1)^s p \text{Det} O_\sigma = -1$  and  $O_\sigma \neq \mathbb{1}$ . In this case,  $E_{n,B}(O_\sigma \mathbf{k}) = -E_{n,B}(\mathbf{k})$  and this implies that the minimum and maximum values of LLS has the same magnitude but opposite in sign, i.e.,  $\max E_{n,B}(\mathbf{k}) = -\min E_{n,B}(\mathbf{k})$ . Notable examples are time-reversal symmetry  $T$  and reflection symmetry  $R$ .

### Symmetry constraint on $\chi_{xy}^{nm}(\mathbf{k})$

Although the symmetry analysis for the modified band dispersion  $E_{n,B}(\mathbf{k})$  is sufficient for studying the Landau level spreading (LLS), the symmetry analysis for  $\chi_{xy}^{nm}(\mathbf{k})$  provides some useful insights for understanding of the LLS as the inter-band coupling. From Eqs. (S3) and (S4), we obtain the relation between  $\chi_{ij}^{nm}(\mathbf{k})$  and  $\chi_{ij}^{nm\sigma}(O_\sigma \mathbf{k})$  where the band  $m$  and the band  $m_\sigma$  are

related by the symmetry  $\sigma$  so that  $\varepsilon_m(\mathbf{k}) = p \varepsilon_{m_\sigma}(O_\sigma \mathbf{k})$ :

$$\begin{aligned}
\chi_{ij}^{nm\sigma}(O_\sigma \mathbf{k}) &= \left[ \langle \partial_{\mathbf{k}'_i} u_n(\mathbf{k}') | u_{m_\sigma}(\mathbf{k}') \rangle \langle u_{m_\sigma}(\mathbf{k}') | \partial_{\mathbf{k}'_j} u_n(\mathbf{k}') \rangle \right]_{\mathbf{k}'=O_\sigma \mathbf{k}} \\
&= [O_\sigma]_{ii'} [O_\sigma]_{jj'} \partial_{i'} \left( e^{i\phi_n(\mathbf{k})} \overline{\langle u_n(\mathbf{k}) \rangle^s} U_\sigma(\mathbf{k})^\dagger \right) \\
&\quad \times \left( U_\sigma(\mathbf{k}) \overline{\langle u_m(\mathbf{k}) \rangle \langle u_m(\mathbf{k}) \rangle^s} U_\sigma(\mathbf{k})^\dagger \right) \partial_{j'} \left( U_\sigma(\mathbf{k}) \overline{\langle u_n(\mathbf{k}) \rangle^s} e^{-i\phi_n(\mathbf{k})} \right) \\
&= [O_\sigma]_{ii'} [O_\sigma]_{jj'} \overline{\chi_{i'j'}^{nm}(\mathbf{k})}^s.
\end{aligned} \tag{S8}$$

Let us now apply Eq. (S8) to i) chiral symmetry  $C$ , ii) space-time-inversion symmetry  $I_{ST}$ , iii) a combined symmetry  $C_{ST} = C \circ I_{ST}$  with  $C$  and  $I_{ST}$ , iv) time-reversal symmetry  $T$ , and v) reflection symmetry

i) Chiral symmetry  $C$  is characterized by  $\mathbf{g}_C = (O_\sigma, s, p) = (\mathbb{1}, 0, -1)$ , and Eq. (S8) implies  $\chi_{ij}^{nm\sigma}(\mathbf{k}) = \chi_{ij}^{nm}(\mathbf{k})$ . Noting that  $\varepsilon_m(\mathbf{k}) = -\varepsilon_{m_\sigma}(\mathbf{k})$ , we obtain

$$\sum_{a=m, m_\sigma} \varepsilon_a(\mathbf{k}) \chi_{ij}^{na}(\mathbf{k}) = 0. \tag{S9}$$

Thus, for each chiral-symmetric pair  $|u_m(\mathbf{k})\rangle$  and  $|u_{m_\sigma}(\mathbf{k})\rangle$ , the contribution to the modified band dispersion  $E_{n,B}(\mathbf{k})$  cancels out.

ii) Space-time inversion  $I_{ST}$  define by  $\mathbf{g}_{I_{ST}} = (\mathbb{1}, 1, 1)$  imposes the condition  $\chi_{ij}^{nm\sigma}(\mathbf{k}) = (\chi_{ij}^{nm}(\mathbf{k}))^*$ . In  $I_{ST}$ -symmetric system, let us suppose non-degenerate band structure with band labeling  $m = m_\sigma$  with  $\varepsilon_m(\mathbf{k}) = \varepsilon_{m_\sigma}(\mathbf{k})$  for simplicity. Hence,

$$\varepsilon_m(\mathbf{k}) \operatorname{Im} \chi_{ij}^{nm}(\mathbf{k}) = 0, \tag{S10}$$

and contribution from each energy eigenstate  $|u_m(\mathbf{k})\rangle$  vanishes.

iii) Let us consider  $C_{ST} = C \circ I_{ST}$ , a combination of chiral and space-time-inversion symmetries, characterized by  $\mathbf{g}_{C_{ST}} = (\mathbb{1}, 1, -1)$ . For this symmetry, the condition  $\chi_{ij}^{nm\sigma}(\mathbf{k}) = (\chi_{ij}^{nm}(\mathbf{k}))^*$  is imposed. This symmetry constraint is similar to  $I_{ST}$ -symmetric system, but now  $\varepsilon_m(\mathbf{k}) = -\varepsilon_{m_\sigma}(\mathbf{k})$ . Hence,

$$\sum_{\{\varepsilon_a(\mathbf{k}) > 0\}} \varepsilon_a(\mathbf{k}) \operatorname{Im} \chi_{ij}^{na}(\mathbf{k}) = \sum_{\{\varepsilon_{\bar{a}}(\mathbf{k}) < 0\}} \varepsilon_{\bar{a}}(\mathbf{k}) \operatorname{Im} \chi_{ij}^{n\bar{a}}(\mathbf{k}). \tag{S11}$$

In this system, both energy eigenstates with positive and negative energy eigenvalues contribute to the LLS with the same sign. In the main text, we discuss the spin-orbit-coupled (SOC) Lieb model. This model possesses  $C_{ST}$ ,

$$C_{ST}H_{socL}(\mathbf{k})C_{ST}^{-1} = -H_{socL}(\mathbf{k}) \quad \text{where} \quad C_{ST} = \text{Diag}(1, -1, 1)\mathcal{K}. \quad (\text{S12})$$

This symmetry leads to  $\chi_{\text{socL},xy}^{\text{fb},+}(\mathbf{k}) = \left(\chi_{\text{socL},xy}^{\text{fb},-}(\mathbf{k})\right)^*$ .

iv) Time-reversal symmetry  $T$  is characterized by  $\mathbf{g}_T = (-1, 1, 1)$ , and  $\chi_{ij}^{nm\sigma}(-\mathbf{k}) = (\chi_{ij}^{nm}(\mathbf{k}))^*$  consequently. Noting that  $\varepsilon_m(\mathbf{k}) = \varepsilon_{m\sigma}(-\mathbf{k})$ , we obtain

$$\varepsilon_m(\mathbf{k}) \text{Im} \chi_{ij}^{nm}(\mathbf{k}) = -\varepsilon_{m\sigma}(-\mathbf{k}) \text{Im} \chi_{ij}^{nm\sigma}(-\mathbf{k}). \quad (\text{S13})$$

Thus,  $E_{n,B}(\mathbf{k}) = -E_{n,B}(-\mathbf{k})$ , and this implies  $\max E_{n,B}(\mathbf{k}) = -\min E_{n,B}(\mathbf{k})$ .

v) For a discussion on reflection symmetry  $R$ , we consider  $R_x$ , characterized by  $\mathbf{g}_{R_x} = (\text{Diag}(-1, 1), 0, 1)$ , for convenience.  $R_x$  imposes  $\chi_{ij}^{nm\sigma}(-k_x, k_y) = -\chi_{ij}^{nm}(\mathbf{k})$ . Considering  $\varepsilon_m(\mathbf{k}) = \varepsilon_{m\sigma}(-k_x, k_y)$ , we obtain

$$\varepsilon_m(\mathbf{k}) \text{Im} \chi_{ij}^{nm}(\mathbf{k}) = -\varepsilon_{m\sigma}(-k_x, k_y) \text{Im} \chi_{ij}^{nm\sigma}(-k_x, k_y), \quad (\text{S14})$$

and  $E_{n,B}(\mathbf{k}) = -E_{n,B}(-k_x, k_y)$ . In similar to iv), we conclude that  $\max E_{n,B}(\mathbf{k}) = -\min E_{n,B}(\mathbf{k})$ .

Let us comment on the case where some bands are degenerate. When the band  $m$  is degenerate with other band(s),  $\chi_{ij}^{nm}(\mathbf{k})$  or  $\varepsilon_m(\mathbf{k}) \text{Im} \chi_{ij}^{nm}(\mathbf{k})$  alone is not gauge invariant. Let us suppose that the  $D$  number of bands, whose band indices are  $m_1, m_2, \dots, m_D$ , form a set of degenerate bands  $\{m\}$ , i.e.,  $(m_1, m_2, \dots, m_D) \in \{m\}$ . Then,  $\sum_{a \in \{m\}} \chi_{ij}^{na}(\mathbf{k})$  and  $\sum_{a \in \{m\}} \varepsilon_a(\mathbf{k}) \text{Im} \chi_{ij}^{na}(\mathbf{k})$  are gauge invariant under the gauge transformation,

$$|u_{m_i}(\mathbf{k})\rangle \rightarrow |u_{m_j}(\mathbf{k})\rangle G_{m_j m_i}(\mathbf{k}) \quad (i, j = 1, 2, \dots, D), \quad (\text{S15})$$

where  $G_{m_j m_i}(\mathbf{k})$  is  $D$ -by- $D$  unitary matrix.

## Supplementary Note 2. Landau level spreading of flat-band system with chiral symmetry

In this section, we discuss the LLS of flat-band system in the presence of chiral symmetry.

As discussed in the main text and Supplementary Note 1, the LLS of chiral-symmetric system is forbidden in finite or all range of magnetic flux. First, let us discuss some properties of chiral-symmetric system in the zero magnetic flux. For chiral-symmetric Hamiltonian, the symmetry relation,

$$CH(\mathbf{k})C^{-1} = -H(\mathbf{k}) \quad (\text{S16})$$

holds. This implies that eigenstates  $|u_a(\mathbf{k})\rangle$  and  $|u_{\bar{a}}(\mathbf{k})\rangle$ , having energy eigenvalues  $\varepsilon_a(\mathbf{k})$  and  $\varepsilon_{\bar{a}}(\mathbf{k}) = -\varepsilon_a(\mathbf{k})$  respectively, are related by the chiral symmetry operator  $C$ :

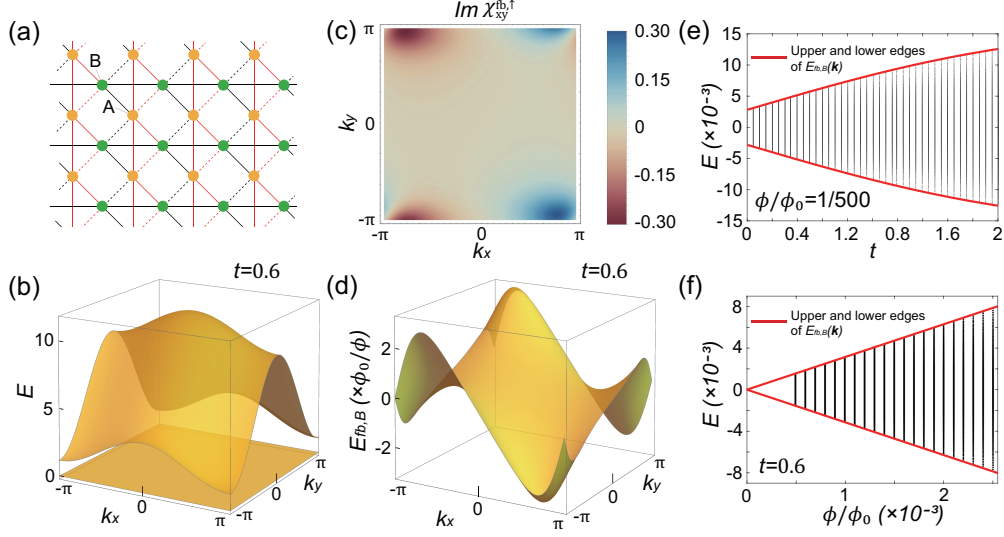
$$C|u_a(\mathbf{k})\rangle = |u_{\bar{a}}(\mathbf{k})\rangle B(\mathbf{k})_{\bar{a}a}. \quad (\text{S17})$$

Here,  $B(\mathbf{k})$  denotes the sewing matrix for the chiral symmetry. The chiral eigenvalues  $c$  are given by the eigenvalues of  $B_{\bar{a}a}(\mathbf{k})$ . When  $\varepsilon_{\bar{a}}(\mathbf{k}) = -\varepsilon_a(\mathbf{k}) \neq 0$ , the sewing matrix is equal to

$$B(\mathbf{k})_{\bar{a}a} = \begin{pmatrix} 0 & 1 \\ 1 & 0 \end{pmatrix}, \quad (\text{S18})$$

up to unitary transformation, and its eigenvalues are given by  $c = \pm 1$ . Conversely, this implies that two degenerate flat-bands with zero energy having opposite chiral eigenvalues  $c = \pm 1$  can be gapped under chiral-symmetric perturbations. However, a set of zero-energy flat bands cannot be gapped when all the chiral eigenvalues of such flat bands are equal. Since the sewing matrix  $B(\mathbf{k})_{\bar{a}a}$  for all bands is identical to the chiral symmetry operator  $C$  up to unitary transformation, the minimum number of zero-energy flat bands, guaranteed to be exists due to the chiral symmetry, is given by  $|\text{Tr}[C]|$ .

In the magnetic finite flux, the system still remains chiral symmetric. This is because chiral symmetry arises from a specific way of choosing the hoppings between the sublattices, and it is not changed by the Peierls substitution. For the magnetic unit cell  $q$  times larger than the original unit cell, the minimal number of flat bands are equal to  $q|\text{Tr}[C]|$  where  $q$  is determined by the magnetic flux  $\frac{\phi}{\phi_0} = q_0 \frac{p}{q}$  ( $q_0, p, q \in \mathbb{Z}$ ). Note that  $q_0$  is a constant dependent on the gauge choice and the models. These zero-energy flat bands still have the same chiral eigenvalues, thus these are protected by chiral symmetry ( $C_{\text{new}} = \bigoplus_{i=1}^q C$  now). Hence, unless a gap between zero-energy and non-zero-energy Landau levels closes as the magnetic flux increases, the LLS is forbidden even in



**Supplementary Figure 1. Landau level spreading of a flat-band system with time-reversal symmetry**  
 (a) Lattice structure for the  $T$ -symmetric checkerboard model. Neighboring sites connected by the same type of bonds (a solid or dotted line) with the same color have the same hopping amplitudes. (b) The band structure of  $H_T(\mathbf{k})$ . (c) Distribution of  $\text{Im} \chi_{xy}^{\text{fb},\uparrow}(\mathbf{k})$ . (d) The modified band dispersion  $E_{\text{fb},B}(\mathbf{k})$  of the flat band in the presence of magnetic flux. (e) Landau level spectra of the flat band (black dots) as a function of  $t$  for magnetic flux  $\phi/\phi_0 = 1/500$ . (f) Landau level spectra of the flat band (black dots) as a function of magnetic flux  $\phi/\phi_0$  for  $t = 0.6$ . (e)-(f) The upper and lower bounds of Landau levels are equal in magnitude but opposite in sign.

the finite magnetic flux when the number of flat bands is  $q|\text{Tr}[C]|$  at the zero magnetic flux. When such a gap closing occurs at  $\frac{\phi}{\phi_0} = \varphi_*$ , the LLS can be finite for the magnetic flux larger than  $\varphi_*$ . Nevertheless, there must be at least the  $q|\text{Tr}[C]|$  number of zero-energy Landau levels.

### Supplementary Note 3. More lattice models

#### Time-reversal-symmetric system on the checkerboard lattice

When a time-reversal symmetry  $T$  exists at zero magnetic field, the LLS of an IFS has the minimum and maximum values of the same magnitude but opposite in sign. We consider a  $T$ -symmetric system defined in the checkerboard lattice. The lattice structure is shown in Supplementary Figure 1(a). The on-site potentials at A- and B-sites are set to be 5 and  $1+t^2$ , respectively. The hopping parameters are set to 2 along the red solid line,  $t$  along the black solid line, 1 along the red dashed lines, and  $2t$  along the black dashed lines. The tight-binding Hamiltonian is written

as

$$H_T(\mathbf{k}) = \begin{pmatrix} 5 + 4 \cos k_y & 2te^{-i\mathbf{k}\cdot\mathbf{d}_1} + 2e^{-i\mathbf{k}\cdot\mathbf{d}_2} + e^{i\mathbf{k}\cdot\mathbf{d}_1} + te^{i\mathbf{k}\cdot\mathbf{d}_2} \\ 2te^{i\mathbf{k}\cdot\mathbf{d}_1} + 2e^{i\mathbf{k}\cdot\mathbf{d}_2} + e^{-i\mathbf{k}\cdot\mathbf{d}_1} + te^{-i\mathbf{k}\cdot\mathbf{d}_2} & 1 + t^2 + 2t \cos k_x \end{pmatrix}, \quad (\text{S19})$$

where  $\mathbf{d}_1 = (1/2, 1/2)$  and  $\mathbf{d}_2 = (-1/2, 1/2)$ . This Hamiltonian gives a zero-energy flat band, and a dispersive band with energy  $\varepsilon_{T,\uparrow}(\mathbf{k}) = 6 + t^2 + 2t \cos k_x + 4 \cos k_y > 0$  as shown in Supplementary Figure 1(b). The time-reversal symmetry operator is given by the complex conjugation  $\mathcal{K}$ , i.e.,  $T = \mathcal{K}$ , which gives a symmetry relation,

$$T H_T(\mathbf{k}) T^{-1} = H_T(-\mathbf{k}). \quad (\text{S20})$$

The analytic form of the fidelity tensor  $\chi_{xy}^{nm}(\mathbf{k})$  is given by

$$\chi_{T,xy}^{\text{fb},\uparrow}(\mathbf{k}) = \frac{(3 + 4i \sin k_y)(t^2 + 2i \sin k_x - 1)}{4 (\varepsilon_{T,\uparrow}(\mathbf{k}))^2}. \quad (\text{S21})$$

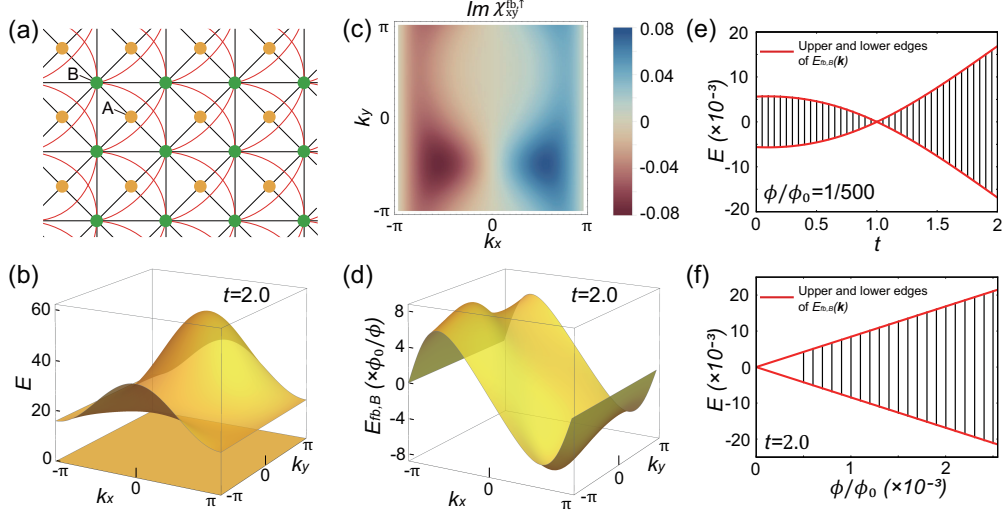
Then, the modified band dispersion for the flat band is given by

$$E_{\text{fb},B}^T(\mathbf{k}) = -\frac{\pi(3t \sin k_x + 2(t^2 - 1) \sin k_y)}{\varepsilon_{T,\uparrow}(\mathbf{k})} \frac{\phi}{\phi_0}. \quad (\text{S22})$$

In Supplementary Figures 1(c)-(d),  $\text{Im } \chi_{T,xy}^{\text{fb},\uparrow}(\mathbf{k})$  and  $E_{\text{fb},B}^T(\mathbf{k})$  are shown. Note that  $E_{\text{fb},B}^T(-\mathbf{k}) = -E_{\text{fb},B}^T(\mathbf{k})$ . Consequently, the Landau levels of the flat band spread in both positive and negative energy directions with the same amounts as shown in Supplementary Figures 1(e)-(f).

### Reflection-symmetric system on the checkerboard lattice

In a similar to time-reversal symmetric system at the zero magnetic field, we expect that the LLS whose the minimum and maximum values have the same magnitude but opposite in sign, for reflection  $R$  symmetric system at the zero field. We consider a  $R$ -symmetric system defined in the checkerboard lattice. This model is symmetric under reflection symmetry  $R$  in the  $x$ -direction. The lattice structure is shown in Supplementary Figure 2(a). The tight-binding Hamiltonian consists of the hopping processes up to the next-to-next neighbor hopping. In momentum space, the



Supplementary Figure 2. **Landau level spreading of a flat-band system with reflection symmetry** (a) The lattice structure for the  $I_{ST}$ -symmetric checkerboard model. The red and black lines denote the hopping processes between  $A$  and  $B$  sublattices. (b) The band structure of  $H_R(\mathbf{k})$  with  $t = 2.0$ . (c) Distribution of  $\text{Im}\chi_{xy}^{\text{fb},\uparrow}(\mathbf{k})$  with  $t = 2.0$ . (d) The modified band dispersion  $E_{\text{fb},B}(\mathbf{k})$  of the flat band in the presence of magnetic flux. (e) Landau level spectra of the flat band (black dots) as a function of  $t$  for magnetic flux  $\phi/\phi_0 = 1/500$ . We note that space-time inversion symmetry  $I_{ST}$  exist when  $t = 1.0$ , thus the LLS is strongly suppressed. (f) Landau level spectra of the flat band (black dots) as a function of magnetic flux  $\phi/\phi_0$  for  $t = 2.0$ . (e)-(f) The upper and lower bounds of Landau levels are equal in magnitude but opposite in sign.

Hamiltonian is written as

$$H_R(\mathbf{k}) = |\phi(\mathbf{k})\rangle\langle\phi(\mathbf{k})|, \quad (\text{S23})$$

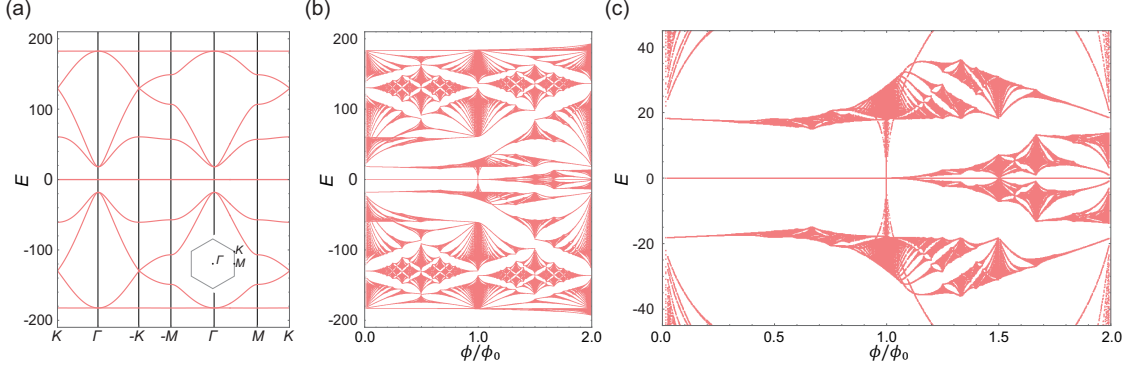
$$|\phi(\mathbf{k})\rangle = (ie^{-i\mathbf{k}\cdot\mathbf{d}_1} + ie^{-i\mathbf{k}\cdot\mathbf{d}_2} + te^{i\mathbf{k}\cdot\mathbf{d}_1} + te^{i\mathbf{k}\cdot\mathbf{d}_2}, 4)^T, \quad (\text{S24})$$

where  $\mathbf{d}_1 = (1/2, 1/2)$  and  $\mathbf{d}_2 = (-1/2, 1/2)$ . The band structure for  $t = 2.0$  is shown in Supplementary Figure 2(b). The flat band's energy is zero and the energies of dispersive band is

$$\varepsilon_{R,\uparrow}(\mathbf{k}) = 18 + 2t^2 + 2(1 + t^2) \cos k_x + 4t \sin k_y + 2t \sin(k_x + k_y) - 2t \sin(k_x - k_y). \quad (\text{S25})$$

The reflection symmetry operator is given by  $R = \text{Diag}(1, 1)$  which gives a symmetry relation,

$$RH_R(\mathbf{k})R^{-1} = H_R(-k_x, k_y). \quad (\text{S26})$$



Supplementary Figure 3. **Landau level spreading of 10-band TBG model** (a) The band structure for 10-band TBG model proposed in Ref. [27]. The Brillouin zone and the high-symmetry points are defined in the inset. (b) The Hofstadter spectrum exhibits the zero LLS of flat band at the magnetic flux  $\frac{\phi}{\phi_0}$  in a range of  $0 \leq \frac{\phi}{\phi_0} < 1$ . When  $\frac{\phi}{\phi_0} = 1$ , a gap closing at  $E = 0$  occurs, then the finite LLS is observed for  $\frac{\phi}{\phi_0} > 1$ . (c) A zoom-in of the Hofstadter spectrum shown in (b). Chiral symmetry guarantees the zero-energy Landau levels despite the appearance of non-zero LLS.

The analytic form of the fidelity tensor  $\chi_{xy}^{nm}(\mathbf{k})$  is given by

$$\chi_{R,xy}^{\text{fb},\uparrow}(\mathbf{k}) = \frac{8i \sin k_x(t^2 + 2i \cos k_y - 1)}{(\varepsilon_{R,\uparrow}(\mathbf{k}))^2}. \quad (\text{S27})$$

Then, the modified band dispersion for the flat band is given by

$$E_{\text{fb},B}^R(\mathbf{k}) = -\frac{16\pi(t^2 - 1) \sin k_x}{\varepsilon_{R,\uparrow}(\mathbf{k})} \frac{\phi}{\phi_0}. \quad (\text{S28})$$

In Supplementary Figures 2(c)-(d),  $\text{Im } \chi_{R,xy}^{\text{fb},\uparrow}(\mathbf{k})$  and  $E_{\text{fb},B}^R(\mathbf{k})$  are shown. Note that  $E_{\text{fb},B}^R(-k_x, k_y) = -E_{\text{fb},B}^R(\mathbf{k})$ . Consequently, the Landau levels of the flat band spread in both positive and negative energy directions with the same amounts as shown in Supplementary Figures 2(e)-(f).

### Ten-band model for twisted bilayer graphene

In this section, we discuss one more example for chiral-symmetric system. For this, we consider the ten-band model for twisted-bilayer graphene (TBG) proposed in Ref. 27. The band structure and the Hofstadter spectrum is shown in Supplementary Figures 3(a) and (b)-(c), respectively. The band structure exhibits two degenerate flat bands at zero energy when the on-site potential is neglected. Moreover, these flat bands have fragile topology protected by  $C_{2z} \circ T$  [9, 10, 27,

[39](#). Although this system is not our interest in this paper as we focus only on an isolated and topologically trivial flat band, we study this system in detail as an important example of chiral-symmetric flat-band system.

As shown in Supplementary Figures [3](#)(b)-(c), There is no LLS in the Hofstadter spectrum for  $0 \leq \frac{\phi}{\phi_0} < 1$ . This is because the chiral symmetry operator of this system is given by

$$C = \text{Diag}(-1, -1, -1, -1, 1, 1, 1, 1, 1, 1), \quad (\text{S29})$$

and  $\text{Tr}[C] \neq 0$  at the zero magnetic field. According to the discussion in Supplementary Note 2, this implies the zero LLS in a finite range of the magnetic flux. Interestingly, the gap near  $E = 0$  closes at  $\frac{\phi}{\phi_0} = 1$ , and then the LLS is developed after the gap closing, as shown in Supplementary Figure [3](#)(c). The connection between the gap closing and fragile topology is discussed in Ref. [11](#).